Research Square

Preprints are preliminary reports that have not undergone peer review.
They should not be considered conclusive, used to inform clinical practice,
or referenced by the media as validated information.

Ilexgenin A promotes cellular senescence through the PI3K/Akt/FOXO1/TXNIP pathway in human non-small cell lung cancer NCI-H460 cells

Xiang-Ke Sun
Loudi Central Hospital of Hunan Province &The First Affiliated Hospital of Guangzhou Medical University Loudi Hospital

Min Yang
Loudi Central Hospital of Hunan Province &The First Affiliated Hospital of Guangzhou Medical University Loudi Hospital

Yu-Yuan Liu
Air force hospital of the southern war zone of the Chinese people's liberation army

Rong-Bo Xu
Luoding People's Hospital

Yong-Rong Zhang
Loudi Central Hospital of Hunan Province &The First Affiliated Hospital of Guangzhou Medical University Loudi Hospital

Tong-Lin Chen
Shantou Hospital of Traditional Chinese Medicine

Jun-Hui Ouyang
13574507026@163.com

Loudi Central Hospital of Hunan Province &The First Affiliated Hospital of Guangzhou Medical University Loudi Hospital

---

Article

Keywords: Ilexgenin A, FOXO1, TXNIP, cellular senescence, NSCLC

Posted Date: July 14th, 2026

DOI: https://doi.org/10.21203/rs.3.rs-10017026/v1

License: This work is licensed under a Creative Commons Attribution 4.0 International License.
Read Full License

Additional Declarations: No competing interests reported.

Abstract

Cellular senescence is closely associated with the progression of non-small cell lung cancer (NSCLC), the most prevalent subtype of lung cancer. Ilexgenin A (IA) is the main bioactive compound isolated from Ilex hainanensis Merr tosis and has been shown to suppress the growth of multiple tumors. However, the effect of IA on NSCLC cell senescence remains unknown. Our results showed that administration of IA induced cellular senescence in human NSCLC cell line NCI-H460, as evidenced by up-regulation of p16 and p21 expression, incremental proportion of SA-β-Gal-positive cells, decreased cellular proliferative capability. Mechanistically, IA inhibited the phosphatidylinositol 3-kinase (PI3K)/Akt signaling pathway, which promoted nuclear translocation of forkhead box O1 (FOXO1) and then transcriptionally activated thioredoxin-interacting protein (TXNIP). In summary, these data suggest that IA stimulates NCI-H460 cell senescence through the PI3K/Akt/FOXO1/TXNIP pathway, thereby providing new theoretical support for its clinical application.

1. Introduction

Lung cancer is regarded as one of the most prevalent and leading causes of cancer-related death across the world, particularly among elderly individuals[1]. It is divided into small cell lung cancer and non-small cell lung cancer (NSCLC), and the latter is estimated to account for more than 80% of cases [2]. NSCLC contains several subtypes, such as adenocarcinoma, squamous cell carcinoma and large cell carcinoma. Because its incidence continues to rise in recent years, NSCLC has become a major public healthy challenge with a considerable burden of economy and society. The majority of NSCLC patients are diagnosed at the metastatic stages and are inoperable, with chemotherapy being the major therapeutic method. Despite advancements in chemotherapy, there are still many challenges in NSCLC patients suffering from chemotherapy, such as high recurrence rate, complications, controversial efficacy, and drug resistance [3, 4]. Therefore, there is an urgent need to reveal the critical molecular mechanisms and develop novel therapeutic strategies for NSCLC.

NSCLC is currently regarded as a multifactorial and complex disease, involving a variety of biological processes. Cellular senescence is a state of irreversible cell cycle block, which is characterized by incremental cytostatic gene expression (primarily p21 and p16), increased senescence-associated β-galactosidase (SA-β-Gal) activity, decreased cellular proliferative ability, and senescence-associated secretory phenotypes [5, 6]. Cellular senescence is generally thought to be a potential mechanism to suppress the development of tumors or enhance the sensitivity of anti-tumor drugs [7]. There is increasing evidence that stimulating NSCLC cell senescence contributes to inhibition of tumorigenesis [8, 9]. Ilexgenin A (IA, Fig. 1A) is a natural pentacyclic triterpene compound extracted from the dry leaves of Ilex hainanensis Merr tosis in southern China. Modern pharmacological studies have demonstrated that IA has multiple beneficial effects, including anti-inflammation, anti-angiogenesis and hypolipidemic property [10, 11]. Of note, IA has been shown to inhibit the progression of hepatocellular carcinoma,

colorectal cancer and melanoma [12–14]. However, the impact of IA on lung cancer, particularly NSCLC cell senescence, remain largely known.

The phosphatidylinositol 3-kinase (PI3K)/Akt signaling pathway is considered to one of the most important oncogenic pathways in human malignant tumors. Extensive research has shown that activation of this pathway inhibits tumor cell senescence and facilitates tumorigenesis [15–17]. Forkhead box O1 (FOXO1) belongs to a member of the FOXO family of transcription factors and functions as a downstream molecular of the PI3K/Akt signaling pathway [18]. Thioredoxin-interacting protein (TXNIP) is an α-arrestin family protein that is known to function as a tumor suppressor. TXNIP plays an important role in promoting cellular senescence [19, 20]. Nevertheless, it is still unclear whether FOXO1 can affect TXNIP gene transcription.

The aim of this study was to observe the influence of IA cellular senescence in human NSCLC cell line NCI-H460 and explore the underlying molecular mechanism. Our results showed that IA exerted a promotive effect on NCI-H460 cell senescence, which was mediated by the PI3K/Akt/FOXO1/TXNIP signaling pathway. To our knowledge, this is the first report establishing a link of IA to NSCLC.

2. Materials and methods

2.1. Cell culture and IA treatment

NCI-H460 cells (#CL-0299, Pricella, Wuhan, China) were maintained in RPMI-1640 medium (#31800, Solarbio, Beijing, China) with 10% fetal bovine serum (#A5669701, Gibco, Grand Island, NE, USA) and 1% penicillin-streptomycin, and were kept under a controlled condition (37 ℃, 5% CO_2). When grown to 70%-80% confluence, cells were treated with IA (#HY-N6255, MedChemExpress, Monmouth Junction, NJ, USA), which was dissolved in dimethylsulfoxide (DMSO; #D2650, Sigma-Aldrich, St. Louis, MO, USA) for the indicated concentrations and durations.

2.2 Detection of cell viability

NCI-H460 cells were seeded in a 96-well plate at a density of approximately 1×10^4 cells per well. Following cell attachment, cells were treated with different concentrations of IA for 24 hours or 40 μM IA for various durations. At the end of the treatment, 10 μL of CCK-8 solution (#C0037, Beyotime, Shanghai, China) was add to each well and then incubated in a cell culture incubator for another 4 hours. The absorbance was measured at 450 nm for each well using a microplate reader. The wells containing cell-free medium were used as blank controls to calculate the relative viability of each cell group compared to the control group.

2.3 Small interfering RNA (siRNA) transfection

To knock down TXNIP and FOXO1, NCI-H460 cells were transfected with the corresponding siRNAs (50 nM) using Lipofectamine™ 3000 (#L3000150, Invitrogen, Carlsbad, CA, USA) when they reached

approximately 80% confluence. After 48 h of transfection, the expression of TXNIP and FOXO1 was measured using quantitative real-time polymerase chain reaction (qRT-PCR) and western blot to determine the transfection efficiency. The siRNAs targeting TXNIP or FOXO1 as well as negative control siRNA (si-NC) were obtained from Sangon Biotech (Shanghai, China). Their sequences are as follows: si-FOXO1 (5'-auaguacuagcauuu gagcttdTdT-3'), si-TXNIP (5'-GAGAAUACAUGUUCCCGAAdTdT-3') and si-NC (5'-UUCUCCGAACGUGU CACGUdTdT-3').

2.4 RNA-sequencing (RNA-seq)

NCI-H460 cells were stimulated with vehicle (DMSO) or IA (40 μM). After 24 hours, cells were collected for RNA-seq (Genewiz, Suzhou, China). Briefly, total RNA was extracted from NCI-H460 cells, which was accompanied by quality control. Qualified samples were used for cDNA library construction, followed by high-throughput sequencing to obtain raw reads (FASTQ files). Data analysis included raw data quality assessment using FastQC-Removal of low-quality sequences via Trimmomatic-Pseudo-alignment of clean reads to the GRCh38 genome by the Salmon software. Subsequently, gene quantification and differential expression analysis were conducted using DESeq2, selecting genes with |log2FoldChange| > 1 and a corrected p-value < 0.05. All statistical analyses and visualizations were completed in the R environment, including volcano plot, heatmap, gene set enrichment analysis (GSEA) and Kyoto Encyclopedia of Genes and Genomes (KEGG) enrichment analysis, with the latter being performed to reveal the major signaling pathways involved in the protective action of IA [21, 22].

2.5 SA-β-Gal staining

Cellular senescence was assessed using a SA-β-galactosidase staining kit. After indicated treatments, NCI-H460 cells were washed with PBS, fixed with the provided fixative for 15 min at room temperature, and washed again. Then, cells were incubated with SA-β-Gal staining solution (#C0602, Beyotime) at 37°C without CO_2 in the dark for 12 hours. SA-β-Gal-positive cells, which were identified by the presence of blue cytoplasmic granules, were imaged under a light microscope. The percentage of senescent NCI-H460 cells was calculated as the ratio of SA-β-Gal-positive cells to total cell number.

2.6 Edu assay

Cell proliferation was assessed using the BeyoClick™ Edu-488 Kit (#C0071S, Beyotime). In brief, NCI-H460 cells were incubated with 50 μM Edu for 2 h at 37°C after indicated treatments, fixed with 4% paraformaldehyde and then permeabilized with 0.3% Triton X-100. After performing the Click reaction for 30 min in the dark, nuclei were counterstained with DAPI (#C0065, Solarbio). The images were visualized under a fluorescence microscope, and the percentage of Edu-positive NCI-H460 cells (green fluorescence) from each group was calculated.

2.7 Bioinformatics prediction and luciferase reporter assay

The UCSC database (http://genome.ucsc.edu/) was employed to search the promoter sequence of TXNIP gene (within the − 2.0 kb fragment upstream of the transcription start site). The FOXO1 binding sites in the TXNIP region was predicted by the JASPAR database (http://jaspar.genereg.net). There were

three putative binding sites, designated as FBS1, FBS2 and FBS3. The TXNIP promoter was produced by PCR against human genomic DNA. The PCR products were separated by agarose gel electrophoresis, and then the DNA fragments were isolated and cloned into the restriction enzyme-digested pGL3 Basic Vector (#E1751, Promega, Madison, WI, USA) using T4 DNA ligase (#EL0011, Thermo Fisher Scientific, Waltham, MA, USA). Mutations were introduced into the FOXO1-binding sites by the QuikChange site-directed mutagenesis kit (#200519, Agilent, Carpinteria, CA, USA). All constructs including TXNIP-WT, FBS1-Mut, FBS2-Mut and FBS3-Mut were verified by sequencing (AuGCT Biotech, Wuhan, China). NCI-H460 cells were co-transfected with each reporter construct and si-NC or si-FOXO1. After 48 hours, cells were harvested to detect the firefly and Renilla luciferase activities using the Dual-Luciferase Reporter Assay System (#E1910, Promega).

2.8 Chromatin immunoprecipitation (ChIP)-qPCR

The ChIP assay was carried out using a ChIP Assay Kit (#P2078, Beyotime) according to the manufacturer's protocol. Briefly, NCI-H460 cells (4×10^6 cells) were included in each ChIP reaction mixture after treatment, underwent crosslinking with 1% formaldehyde and then were stopped by adding glycine solution. Subsequently, DNA fragments were obtained using sonication, followed by immunoprecipitation using the following antibodies: anti-FOXO1 (#18592-1-AP, Proteintech, Chicago, IL, USA) and anti-normal rabbit IgG (#2729S, Cell Signaling Technology, MA, USA). DNA was eluted and purified for qPCR analysis. The sequences of ChIP-qPCR primers are as follows: FBS1 (Forward: 5'-ATTGTTCCTTCAAACAGGTG-3', Reverse: 5'-CTCTTTCTTGTC TCCATCCC-3'), FBS2 (Forward: 5'-CCCCAACTTTGCAGGTAGAA-3', Reverse: 5'-GCGTGC CTGTGCTGTTCGTC – 3'), and FBS3 (Forward: 5'-CTCCAGAGCGCAACAACCAT-3', Reverse: 5'-CAAGCAGGAGG CGGAAACGT-3').

2.9 Molecular docking

The dimensional structural of IA (Compound CID: 21672638) was retrieved from the PubChem databases (https://pubchem.ncbi.nlm.nih.gov). PI3K target protein structure (PDB code: 7BL1) was obtained from the Protein Data Bank (https://www.rcsb.org/). Semi-flexible molecular docking was performed using CB-DOCK2, and the conformation with the lowest binding energy was selected as the optimal binding pose. Visualization and analysis of the docking interactions were performed using PyMOL. The hydrogen bond interaction forces (less than 3.5 angstroms) were labeled.

2.10 RNA extraction and qRT-PCR

Total cellular RNA was extracted using the Trizol method. Briefly, after cell collection, Trizol (#R411-01, Vazyme, Nanjing, China) was added for lysis. RNA pellets were obtained through chloroform layer separation, isopropanol precipitation, and 75% ethanol washing. Concentration and purity were assessed using Nanodrop (ideal A260/A280 ratio between 1.8-2.0), with integrity verified via agarose gel electrophoresis. Subsequently, 1 μg of total RNA was used to synthesize cDNA with a reverse transcription kit. The qRT-PCR reaction system typically comprised 20 μL, including cDNA template, specific primers, and SYBR Green premix (#E347, Novoprotein, China). The reaction protocol is as follows: 30-second pre-denaturation at 95℃, followed by 40 cycles (5 seconds at 95 ℃, 30 seconds at

60 ℃). GAPDH was used as the reference gene, and the relative expression levels of target genes were calculated using the $2^{-\Delta\Delta Ct}$ method. The primer sequences in this study are listed in Table 1. All experiments are performed in triplicate to ensure data reliability.

Table 1
The sequences of primers for qRT-PCR analysis

Genes	Forward primer (5' to 3')	Reverse primer (5' to 3')
IL6	CCTGACCCAACCACAAATGC	AACAATCTGAGGTGCCCATG
TXNIP	GAGAAGAGCCAATTTAACAAAC	TAAGCAAAGATGACCGTAGA
FOXO1	ATACTTCATCTCATTCTCCCTT	ATTCCATTTGCTACCCATC
CDKN2A	TTTGTGGGTTTGTAGAAGCAGG	CGAAGGCGTGAAGATGTGGC
CDKN1A	TTAGCAGCGGAACAAGGAGT	ACGTTAGTGCCAGGAAAGACA
IFNL1	CCGTGGTGCTGGTGACTTTG	AGGCGTCCCTGGCCTTCTTG
GAPDH	GGGTGATGCTTTTCCTAGATT	AATGAAGGGGTCATTGATGG

2.11 Protein extraction and western blot analysis

Total proteins were extracted from cells using RIPA lysis buffer (Novoprotein, China) supplemented with protease and phosphatase inhibitors to preserve protein integrity. Protein quantification was performed using the BCA method to ensure consistent loading volumes. Following denaturation, protein samples were loaded onto SDS-polyacrylamide gels for electrophoresis and separated at a constant voltage. Following electrophoresis, proteins are transferred to polyvinylidene fluoride membranes (Millipore, Billerica, MA, USA). The membranes were blocked with TBST containing 5% skim milk and then incubated overnight at 4°C with the specific primary antibodies (dilution at 1:1000) against p16 (#R23897, Zenbio, Chengdou, China), p21 (#R381102, Zenbio), TXNIP (R382206, Zenbio), FOXO1 (#18592-1-AP, Proteintech), PI3K (#TMAB-01535, Targetmol, Shanghai, China), Akt (#R381117, Zenbio), p-Akt (ser473; #R381555, Zenbio), and β-action (#R380624, Zenbio). After washing, the membranes were incubated at room temperature for 1 hour with horseradish peroxidase-conjugated secondary antibody (1:5000, #ab7090, Abcam, Cambridge, UK). Finally, signals were detected using ECL chemiluminescent reagents. Bands were captured via an imaging system, and grayscale values were analyzed using ImageJ software to quantify target protein expression. β-action served as an internal control to ensure data reliability.

2.12 Determination of subcellular distribution of FOXO1

The subcellular distribution of FOXO1 was determined by western blot and immunofluorescence staining. NCI-H460 cells were incubated with DMSO or IA (20 or 40 μM) for 24 h. Thereafter, cells were harvested, and the proteins in cytoplasmic and nuclear fractions were isolated by using the Nuclear and Cytoplasmic Protein Extraction Kit (#P0027, Beyotime) according to the manufacturer's instructions. β-

action (#R380624, Zenbio) was employed as the endogenous cytoplasmic control, whereas histone H3 (#YT2163, Immunoway, USA) served as the endogenous nuclear control. The relative distribution of FOXO1 was measured by western blot analysis. For immunofluorescence staining, NCI-H460 cells were fixed in 4% paraformaldehyde after indicated treatments. To suppress nonspecific binding, cells were blocked with 5% bovine serum albumin (#A3912, Sigma-Aldrich) at room temperature for 30 min. Then, cells were incubated with the primary antibody against FOXO1 (#18592-1-AP, Proteintech) at 4°C for 12 h. Next, cells were incubated with Cy3-labeled secondary antibody (#SA00009-2, Proteintech) at 37°C in the dark for 30 min. Nuclei were counterstained with DAPI, and images were obtained by a fluorescence microscope.

2.13 Statistical analysis

All experiments were conducted at least three times. The results are presented as the mean ± standard deviation (SD). Statistical analysis was performed by GraphPad Prism 8.0 software (San Diego, CA, USA). An unpaired two-tailed Student's *t*-test was used to compare the differences between two groups. Multiple comparisons were made among ≥ three groups using one-way ANOVA followed by Tukey's test. A *P* value less than 0.05 was considered statistically significant.

3. Results

3.1. IA induces cellular senescence in NCI-H460 cells

To select the optimal treatment concentration and time of IA, the CCK-8 assay was performed to test the effect of IA on cell viability. NCI-H460 cells were treated with various concentrations of IA (0, 10, 20, 40, 60, and 80 μM) for 24 h. The CCK-8 result showed that cell viability was significantly decreased when IA concentrations were higher than 60 μM, whereas there was no cytotoxicity with IA concentrations at 10–40 μM (Fig. 1B). Thereafter, NCI-H460 cells were incubated with 40 μM IA for different durations (0, 6, 12, 24, and 48 h). As illustrated in Fig. 1B, there was no significant alteration in cell viability after 6–24 h of IA treatment, while cytotoxicity appeared when cells were exposed to 40 μM IA for 48 h. Thus, in the subsequent experiments, NCI-H460 cells were treated with IA at 20 (IA-L) or 40 (IA-H) μM for 24 h.

Next, NCI-H460 cells were incubated with 40 μM of IA for 24 h, followed by measurement of RNA-seq. As revealed by the KEGG analysis (Fig. 1C), cell senescence was highly enriched after IA-H treatment. This indicates that IA may be involved in the regulation of NCI-H460 cell senescence. Moreover, GSEA showed that cellular senescence was up-regulated by IA-H (Fig. 1D), implicating that IA may exert a promotive effect on NCI-H460 cellular senescence. To validate the results of RNA-seq, we treated NCI-H460 cells with 20 or 40 μM of IA for 24 h to assess the indicators of cellular senescence. As expected, administration of IA up-regulated the expression of p21 and p16 in a concentration-dependent manner (Fig. 2E), two major molecular markers of cellular senescence. Consistently, the proportion of SA-β-Gal-positive cells was higher in IA-treated cells than that in control cells (Fig. 2F). Decrease in cell proliferation ability is a significant feature of senescent cells. The Edu staining result showed that cell

proliferation was significantly inhibited by IA treatment (Fig. 2G). Collectively, these findings suggest that IA can promote NCI-H460 cell senescence.

3.2. IA induces NCI-H460 cell senescence by up-regulating TXNIP expression

To elucidate the underlying molecular mechanism for IA-induced NCI-H460 cell senescence, we analyzed the data of RNA-seq and found that a total of 1080 genes were differentially expressed between two groups. Among these, 375 genes were up-regulated and 705 genes were down-regulated in IA-H group compared with control group (Fig. 2A and B). The qRT-PCR result further confirmed that TXNIP was the most significantly up-regulated gene (Fig. 2C). Similarly, the protein levels of TXNIP were significantly increased in NCI-H460 cells treated with 40 μM of IA for 24 h (Fig. 2D). Then, NCI-H460 cells were transfected with si-NC or si-TXNIP for 48 h. Efficient knockdown of TXNIP was confirmed by qRT-PCR and western blot (Fig. 2E). Finally, NCI-H460 cells were transfected with si-TXNIP for 48 h, followed by treatment with 40 μM of IA for 24 h. Pretreatment with si-TXNIP significantly reversed IA-induced enhancement of p21 and p16 expression (Fig. 2F). Also, knockdown of TXNIP abolished the effect of IA on SA-β-Gal activity (Fig. 2G). To summarize, IA contributes to NCI-H460 cell senescence in a TXNIP-dependent manner.

3.3. Identification of FOXO1 as a transcriptional activator of TXNIP

FOXO1 is a transcription factor that is broadly expressed in cells and tissues. To reveal the relationship between FOXO1 and TXNIP, we searched for potential FOXO1-binding sites in the TXNIP promoter (within the − 2.0 kb fragment upstream of the transcription start site) by using the JASPAR database. There were three binding sites, designated as FBS1, FBS2 and FBS3 in the TXNIP promoter region (Fig. 3A). To verify the result of bioinformatics prediction. We knocked down FOXO1 (Fig. 3B), and then performed a luciferase reporter assay. Silencing of FOXO1 dramatically decreased transcriptional activity of TXNIP-WT, FBS1-Mut and FBS2-Mut but not FBS3-Mut (Fig. 3C). The ChIP-qPCR assay further showed that there was a direct interaction between FOXO1 and FBS3 but not FBS1 and FBS2 (Fig. 3D). The above results indicate that FBS3 serves as the binding site of FOXO1 in the TXNIP promoter. Notably, the nucleotide sequence of FBS3 was highly conserved across various species, including human, mouse and rat (Fig. 3E). In addition, FOXO1 knockdown markedly decreased the mRNA and protein levels of TXNIP in NCI-H460 cells (Fig. 3F). These data suggest that FOXO1 can transcriptionally activate TXNIP by binding to FBS3.

3.4. IA promotes FOXO1 nuclear translocation and TXNIP transcription

FOXO1 shuttles between the nucleus and the cytoplasm to modulate various biological functions. After entering the nucleus, FOXO1 is able to activate gene transcription. Given that IA did not alter FOXO1

expression (Fig. 2C), we speculated that IA might influence its subcellular distribution. To verify this speculation, NCI-H460 cells were treated with 20 or 40 μM of IA for 24 h. As expected, administration of IA decreased FOXO1 expression at the protein level in the cytoplasm but elevated its content in the nucleus in a concentration-dependent manner (Fig. 4A). Furthermore, immunofluorescence staining showed that IA-L and IA-H dramatically promoted nuclear accumulation of FOXO1 (Fig. 4B). In addition, treatment with IA concentration-dependently increased the transcriptional activity of TXNIP (Fig. 4C). Concomitantly, the binding of FOXO1 to the TXNIP promoter was enhanced by IA (Fig. 4D). Altogether, these data support the notion that IA facilitates the transport of FOXO1 from the cytoplasm to the nucleus and stimulates TXNIP transcription.

3.5. FOXO1 is involved in IA-induced NCI-H460 cell senescence

Since the above studies have demonstrated that IA promotes FOXO1 nuclear translocation and FOXO1 transactivates TXNIP, we next wondered whether FOXO1 was involved in the induction of NCI-H460 cell senescence by IA. To this end, NCI-H460 cells were transfected with si-FOXO1 prior to IA (40 μM) treatment. As shown in Fig. 5A, silencing of FOXO1 significantly reversed IA-induced up-regulation of p16 and p21 expression. The increase in the proportion of SA-β-Gal-positive cells by IA-H was suppressed by FOXO1 knockdown (Fig. 5B). Thus, these observations provide sufficient evidence supporting the involvement of FOXO1 in IA-induced NCI-H460 cell senescence.

3.6. IA inhibits the PI3K/Akt signaling pathway

FOXO1 is a downstream effector of the PI3K/Akt signaling pathway. By analyzing RNA-seq data, we found that the PI3K/Akt signaling pathway was enriched (Fig. 1C). We then incubated NCI-H460 cells with 20 or 40 μM of IA for 24 h. Our results showed that IA concentration-dependently suppressed PI3K expression and reduced the phosphorylated levels of Akt, as evidenced by western blot (Fig. 6A). Finally, molecular docking was performed to predict the binding of IA to PI3K. As demonstrated in Fig. 6B, IA had hydrogen bond interactions with amino acid residues Gln291, Arg690, Glu852, Arg849 and Gln846 on the PI3K domain, with a lower docking score (-13.6 kcal/mol). These findings reveal that IA can combine stably with PI3K and consequently inactivate the PI3K/Akt signaling pathway.

4. Discussion

Currently, NSCLC remains a great threat for human health, with high incidence, poor prognosis and limited therapeutic options. IA, a main bioactive ingredient isolated from Ilex hainanensis Merr tosis, has an anti-tumor property. Cellular senescence refers to a persistent arrest of the cell cycle and is divided into replicative senescence and premature senescence. The induction of tumor cell senescence has emerged as a novel and promising avenue for anti-cancer therapy [23]. However, it is still unclear whether IA is able to promote cellular senescence in NSCLC. In this study, we found that treatment of NCI-H460 cells with IA up-regulated p16 and p21 expression, enhanced the proportion of SA-β-Gal-positive cells

and inhibited cell proliferation in a concentration-dependent manner, suggesting IA as a driver of NCI-H460 cell senescence. To the best of our knowledge, this is the first evidence to reveal the involvement of IA in cellular senescence, broadening our understanding of the biological effects of IA.

TXNIP is a well-known tumor suppressor. It has been demonstrated that TXNIP expression is lower in human NSCLC tissues than surrounding normal tissues [24]. TXNIP suppresses the progression of NSCLC by blocking nuclear factor-κB activation and reducing autophagy [25]. Circ6834 upregulates TXNIP expression by sponging miR-873-5p, leading to inhibition of NSCLC cell growth and metastasis[26]. Conversely, overexpression of miR-411-5p accelerates cell proliferation and migration but impedes cell apoptosis by directly targeting TXNIP in NSCLC cell lines[27]. Methyltransferase-like protein 14 (METTL14) promotes the conversion of pri-miR-93-5p to miR-93-5p by mediating the N6-methyladenosine modification of pri-miR-93-5p. Elevated miR-93-5p downregulates TXNIP expression by binding to its 3'-untranslated region and consequently facilitates the proliferation, migration, invasion and metastasis of NSCLC cells [28]. It is worth noting that TXNIP functions as a driver of cellular senescence in multiple cell types, such as endothelial cells and pancreatic β cells[19, 20]. In the present study, we observed a significant increase of TXNIP expression in IA-treated NCI-H460 cells. Moreover, the promotive effect of IA on NCI-H460 cell senescence was reversed by siRNA-mediated knockdown of TXNIP, suggesting the involvement of TXNIP in IA-induced NCI-H460 cell senescence.

FOXO1, a transcription factor that is often inactivated by nuclear export, serves as a tumor suppressor in many malignancies. FOXO1 was shown to sensitize NSCLC cells to cisplatin-induced apoptosis[29]. Knockdown of silent information regulator type-1 inhibits the progression of NSCLC by activating FOXO1[30]. In contrast, circHERC1 sequesters FOXO1 in the cytoplasm by binding directly to FOXO1, which promotes the proliferation, invasion and metastasis of NSCLC cells[31]. In the current study, we found that IA facilitated the transport of FOXO1 from the cytoplasm to the nucleus. Nuclear accumulation of FOXO1 transcriptionally activated TXNIP, which is consistent with a previous report[32]. FOXO1 has been shown to stimulate cellular senescence in a variety of cell types, including hepatocellular carcinoma cells, ovarian cancer cells and myoblasts[33–35]. Consistent with these findings, siRNA-mediated FOXO1 knockdown abolished IA-induced increase in TXNIP expression and NCI-H460 cell senescence. Thus, our data imply that IA promotes TXNIP expression and NCI-H460 cell senescence in a FOXO1-dependent manner.

The PI3K/Akt signaling pathway participates in a wide range of physiological and pathological processes, such as cellular proliferation, apoptosis, pyroptosis, autophagy and senescence [36]. This pathway is frequently hyperactivated in NSCLC and contributes to tumorigenesis[37, 38]. Activation of the PI3K/Akt signaling pathway can sequesters FOXO1 in the cytoplasm, leading to reduced nuclear accumulation[39]. In a previous study, IA has been reported to inhibit the PI3K/Akt signaling pathway to alleviate atherosclerosis[40]. Similarly, our data showed that IA had a direct interaction with PI3K, and that administration of IA down-regulated PI3K expression and blocked Akt phosphorylation in NCI-H460 cells.

This disruption in the PI3K/AKT axis was accompanied by increased FOXO1 levels in the nucleus. Thus, inactivation of the PI3K/AKT signaling is critical for IA-driven nuclear entry of FOXO1.

Despite this study has clearly demonstrated an inductive effect of IA on NCI-H460 cell senescence, several limitations should be noticed. Firstly, given the complexity of pharmacological effects of IA, other pathways may be involved in IA-induced NCI-H460 cell senescence besides the mentioned above mechanism. Secondly, TXNIP can also bind to nucleotide-binding oligomerization domain-like receptor protein 3 (NLRP3) for promoting NLRP3 inflammasome formation and pyroptosis[41]. Induction of cellular pyroptosis has been proved to enhance drug sensitivity and inhibit NSCLC progression[42, 43]. Whether IA is able to stimulate NCI-H460 cell pyroptosis remains unclear and needs to be determined in future research. Thirdly, we did not establish an animal model to assess the influence of IA on NSCLC cell senescence *in vivo* and this was our future work.

In summary, our findings demonstrate a link between the natural compound IA and NCI-H460 cell senescence, which is involved in a deregulated PI3K/Akt/FOXO1/TXNIP signaling axis (Fig. 7). These findings improve our understanding for the anti-cancer activity of IA and provide new theoretical support for its use as a therapeutic agent against malignant tumors, including NSCLC.

Declarations

Conflicts of interest

The authors declare they do not have anything to disclose regarding conflicts of interest with respect to this manuscript.

Funding

This study was financially supported by the 2024 Loudi City Science and Technology Innovation Plan Project in China (Grant Number: 55).

Author Contribution

X.S. and M.Y. contributed equally to this work. X.S. conceptualized the study and designed the methodology; M.Y. performed the experiments and collected the data, acquired funding; Y.L. and R.X. conducted the formal analysis and data curation; Y.Z. and T.C. validated the results and prepared the original figures and tables; J.O. supervised the project, and revised the manuscript critically for important intellectual content. All authors reviewed and approved the final manuscript.

Acknowledgement

This study was financially supported by the 2024 Loudi City Science and Technology Innovation Plan Project in China (Grant Number: 55).

Data Availability

All data generated or analysed in this study are included in this published article. Raw RNA-seq data that we analysed during the current study are available from sequence read archive (SRA), NCBI BioProject under the accession number PRJNA1482741 (https://www.ncbi.nlm.nih.gov/sra/PRJNA1482741).

References

1. Sung, H. et al. Global Cancer Statistics 2020: GLOBOCAN Estimates of Incidence and Mortality Worldwide for 36 Cancers in 185 Countries. *Cancer J. Clin.* **71**, 209–249. 10.3322/caac.21660 (2021).
2. Jemal, A. et al. Global cancer statistics. *Cancer J. Clin.* **61**, 69–90. 10.3322/caac.20107 (2011).
3. Meyer, M. L. et al. New promises and challenges in the treatment of advanced non-small-cell lung cancer. *Lancet* **404**, 803–822. 10.1016/s0140-6736(24)01029-8 (2024).
4. Stuschke, M. & Pöttgen, C. Effectiveness of adjuvant chemotherapy for resected NSCLC. *Nat. Reviews Clin. Oncol.* **7**, 613–614. 10.1038/nrclinonc.2010.165 (2010).
5. Roger, L., Tomas, F. & Gire, V. Mechanisms and Regulation of Cellular Senescence. *Int. J. Mol. Sci.* **22**, 13173. 10.3390/ijms222313173 (2021).
6. Lucas, V., Cavadas, C. & Aveleira, C. A. Cellular Senescence: From Mechanisms to Current Biomarkers and Senotherapies. *Pharmacol. Rev.* **75**, 675–713. 10.1124/pharmrev.122.000622 (2023).
7. Wang, L., Lankhorst, L. & Bernards, R. Exploiting senescence for the treatment of cancer. *Nat. Rev. Cancer*. **22**, 340–355. 10.1038/s41568-022-00450-9 (2022).
8. Liu, J. et al. Anti-tumor effects of Skp2 inhibitor AAA-237 on NSCLC by arresting cell cycle at G0/G1 phase and inducing senescence. *Pharmacol. Res.* **181**, 106259. 10.1016/j.phrs.2022.106259 (2022).
9. Wang, L. et al. Bortezomib induces cellular senescence in A549 lung cancer cells by stimulating telomere shortening. *Hum. Exp. Toxicol.* **41**, 096032712211240. 10.1177/09603271221124094 (2022).
10. Sun, W. et al. Ilexgenin A, a novel pentacyclic triterpenoid extracted from Aquifoliaceae shows reduction of LPS-induced peritonitis in mice. *Eur. J. Pharmacol.* **797**, 94–105. 10.1016/j.ejphar.2017.01.019 (2017).
11. Zhou, Q. et al. Ilexgenin A inhibits lipid accumulation in macrophages and reduces the progression of atherosclerosis through PTPN2/ERK1/2/ABCA1 signalling pathway. *Biochimica et Biophys. Acta (BBA) - Mol. Cell. Biology Lipids* **1869**, 159533 (2024), 10.1016/j.bbalip.2024.159533

12. Yang, H. et al. Ilexgenin A exerts anti-inflammation and anti-angiogenesis effects through inhibition of STAT3 and PI3K pathways and exhibits synergistic effects with Sorafenib on hepatoma growth. *Toxicol. Appl. Pharmcol.* **315**, 90–101. 10.1016/j.taap.2016.12.008 (2017).
13. Zhang, L. et al. Ilexgenin A prevents early colonic carcinogenesis and reprogramed lipid metabolism through HIF1α/SREBP-1. *Phytomedicine* **63**, 153011 (2019), 10.1016/j.phymed.2019.153011
14. Yang, H. et al. Ilexgenin A induces B16-F10 melanoma cell G1/S arrest in vitro and reduces tumor growth in vivo. *Int. Immunopharmacol.* **24**, 423–431. 10.1016/j.intimp.2014.12.040 (2015).
15. Wang, X., Han, L., Zhang, J., Xia, Q. & Down-Regulated NRSN2 Promotes Cell Proliferation and Survival Through PI3K/Akt/mTOR Pathway in Hepatocellular Carcinoma. *Dig. Dis. Sci.* **60**, 3011–3018. 10.1007/s10620-015-3736-3 (2015).
16. Wu, Y. et al. Saikosaponin A induces cellular senescence in triple-negative breast cancer by inhibiting the PI3K/Akt signalling pathway. *Front. Pharmacol.* **16** 10.3389/fphar.2025.1532579 (2025).
17. Fei, D. et al. Circular RNA ACVR2A promotes the progression of hepatocellular carcinoma through mir-511-5p targeting PI3K-Akt signaling pathway. *Mol. Cancer*. **23** 10.1186/s12943-024-02074-z (2024).
18. Xing, Y. Q. et al. The regulation of FOXO1 and its role in disease progression. *Life Sci.* **193**, 124–131. 10.1016/j.lfs.2017.11.030 (2018).
19. Chen, Q. et al. REDD1 knockdown ameliorates endothelial cell senescence through repressing TXNIP-mediated oxidative stress. *Mech. Ageing Dev.* **221**, 111962. 10.1016/j.mad.2024.111962 (2024).
20. Li, Y. et al. TXNIP Exacerbates the Senescence and Aging-Related Dysfunction of β Cells by Inducing Cell Cycle Arrest Through p38-p16/p21-CDK-Rb Pathway. *Antioxid. Redox. Signal.* **38**, 480–495. 10.1089/ars.2021.0224 (2023).
21. Kanehisa, M. & Goto, S. K. E. G. G. Kyoto Encyclopedia of Genes and Genomes. *Nucleic Acids Res.* **28**, 27–30. 10.1093/nar/28.1.27 (2000).
22. Kanehisa, M., Sato, Y., Kawashima, M., Furumichi, M. & Tanabe, M. KEGG as a reference resource for gene and protein annotation. *Nucleic Acids Res.* **44**, D457–D462. 10.1093/nar/gkv1070 (2016).
23. Nardella, C., Clohessy, J. G., Alimonti, A. & Pandolfi, P. P. Pro-senescence therapy for cancer treatment. *Nat. Rev. Cancer*. **11**, 503–511. 10.1038/nrc3057 (2011).
24. Kopantzev, E. P. et al. Differences in gene expression levels between early and later stages of human lung development are opposite to those between normal lung tissue and non-small lung cell carcinoma. *Lung Cancer*. **62**, 23–34. 10.1016/j.lungcan.2008.02.011 (2008).
25. Kim, J. Y. et al. TXNIP Suppresses Lung Cancer Progression by Inhibiting TRAF6-Mediated NF-κB Activation and Autophagy. *Immune Netw.* **25** 10.4110/in.2025.25.e33 (2025).
26. Wang, M. et al. Circ6834 suppresses non-small cell lung cancer progression by destabilizing ANHAK and regulating miR-873-5p/TXNIP axis. *Mol. Cancer*. **23** 10.1186/s12943-024-02038-3 (2024).

27. Zhang, C. et al. Oncogenic microRNA-411 promotes lung carcinogenesis by directly targeting suppressor genes SPRY4 and TXNIP. *Oncogene* **38**, 1892–1904. 10.1038/s41388-018-0534-3 (2019).
28. Qian, S., Liu, J., Liao, W. & Wang, F. METTL14 drives growth and metastasis of non-small cell lung cancer by regulating pri-miR-93-5p maturation and TXNIP expression. *Genes Genomics*. **46**, 213–229. 10.1007/s13258-023-01436-z (2024).
29. Sun, T. et al. FOXO1 and FOXO3a sensitize non-small-cell lung cancer cells to cisplatin-induced apoptosis independent of Bim. *Acta Biochim. Biophys. Sin.* **52**, 1348–1359. 10.1093/abbs/gmaa129 (2020).
30. Chen, J., Chen, K., Zhang, S. & Huang, X. SIRT1 silencing ameliorates malignancy of non-small cell lung cancer via activating FOXO1. *Sci. Rep.* **14** 10.1038/s41598-024-70970-x (2024).
31. Cui, Y. et al. CircHERC1 promotes non-small cell lung cancer cell progression by sequestering FOXO1 in the cytoplasm and regulating the miR-142-3p-HMGB1 axis. *Mol. Cancer*. **22** 10.1186/s12943-023-01888-7 (2023).
32. Noblet, B. et al. Dual regulation of TxNIP by ChREBP and FoxO1 in liver. *iScience* 24, 102218 (2021). 10.1016/j.isci.2021.102218
33. Chand, V., Liao, X., Guzman, G., Benevolenskaya, E. & Raychaudhuri, P. Hepatocellular carcinoma evades RB1-induced senescence by activating the FOXM1–FOXO1 axis. *Oncogene* **41**, 3778–3790. 10.1038/s41388-022-02394-8 (2022).
34. Diep, C. et al. Progesterone receptors induce FOXO1-dependent senescence in ovarian cancer cells. *Cell. Cycle*. **12**, 1433–1449. 10.4161/cc.24550 (2013).
35. Bae, J. H. et al. ZNF746/PARIS overexpression induces cellular senescence through FoxO1/p21 axis activation in myoblasts. *Cell Death Dis.* **11** 10.1038/s41419-020-2552-7 (2020).
36. Jafari, M., Ghadami, E., Dadkhah, T. & Akhavan-Niaki, H. PI3k/AKT signaling pathway: Erythropoiesis and beyond. *J. Cell. Physiol.* **234**, 2373–2385. 10.1002/jcp.27262 (2019).
37. Tan, A. C. Targeting the PI3K/Akt/mTOR pathway in non-small cell lung cancer (NSCLC). *Thorac. Cancer*. **11**, 511–518. 10.1111/1759-7714.13328 (2020).
38. Wang, S. et al. PTPRH promotes the progression of non-small cell lung cancer via glycolysis mediated by the PI3K/AKT/mTOR signaling pathway. *J. Translational Med.* **21** 10.1186/s12967-023-04703-5 (2023).
39. Nageswaran, V. et al. Gut Microbial Metabolite Imidazole Propionate Impairs Endothelial Cell Function and Promotes the Development of Atherosclerosis. *Arterioscler. Thromb. Vasc. Biol.* **45**, 823–839. 10.1161/atvbaha.124.322346 (2025).
40. Liu, C. et al. A novel pentacyclic triterpenoid, Ilexgenin A, shows reduction of atherosclerosis in apolipoprotein E deficient mice. *Int. Immunopharmacol.* **40**, 115–124. 10.1016/j.intimp.2016.08.024 (2016).
41. Choi, E. H., Park, S. J. & TXNIP A key protein in the cellular stress response pathway and a potential therapeutic target. *Exp. Mol. Med.* **55**, 1348–1356. 10.1038/s12276-023-01019-8 (2023).

42. Liu, Q. et al. Glutamine transporter inhibitor enhances the sensitivity of NSCLC to trametinib through GSDME-dependent pyroptosis. *Biochem. Pharmacol.* **233**, 116796. 10.1016/j.bcp.2025.116796 (2025).

43. Hou, Y. et al. Sophaline B inhibits non-small cell lung cancer by activating NLRP3/caspase-1/GSDMD-dependent pyroptosis and PI3K/AKT/mTOR-mediated autophagy. *Nat. Prod. Res.* **40**, 3015–3027. 10.1080/14786419.2024.2448839 (2026).

Figures

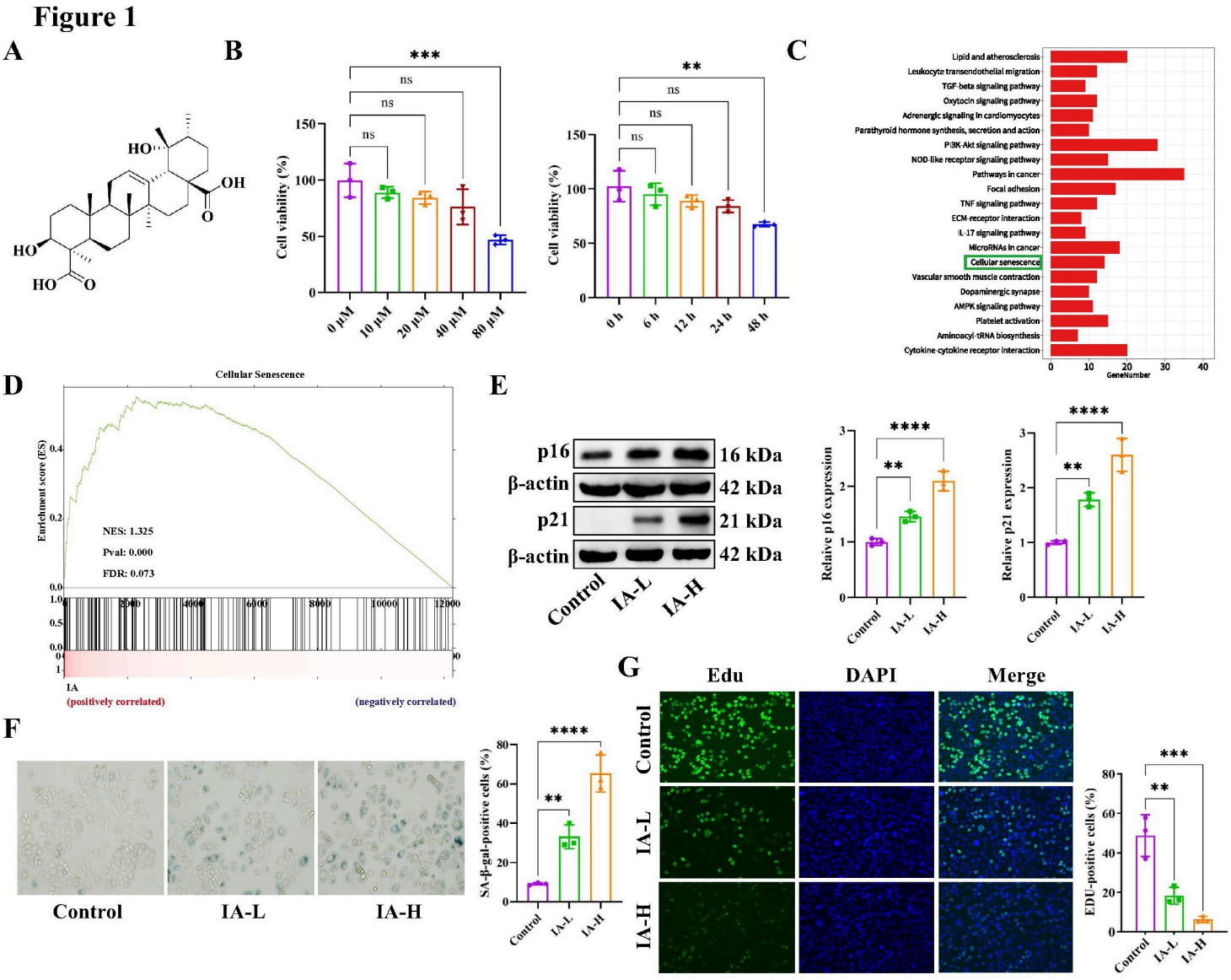


Figure 1

The promotive effect of IA on NCI-H460 cell senescence.

(A) Chemical structure of IA. (B) Cell viability was measured by the CCK-8 assay in NCI-H460 cells treated with IA at the different concentrations and time periods. (C) KEGG pathway enrichment analysis in IA (40 mM)-treated NCI-H460 cells and control cells. The pathway map was generated using Pathview via bioinformatics.com.cn, with copyright being obtained from Kanehisa Laboratories. (D) Gene set enrichment analysis of regulated genes in IA (40 mM)-treated NCI-H460 cells compared with control cells. (E) NCI-H460 cells were treated with 20 or 40 mM of IA for 24 h. Protein samples were immunoblotted with antibodies against p21 or p16, with β-actin as a loading control. (F) Representative images of SA-b-Gal staining and quantitative analysis of positive-stained cells (scale bar=100 mm). (G) Representative Edu staining images and quantification of positive-stained cells (scale bar=100 mm). All data are presented as mean ± SD from three independent experiments. $^{**}P < 0.01$, $^{***}P < 0.001$, $^{****}P < 0.0001$, ns: not significant.

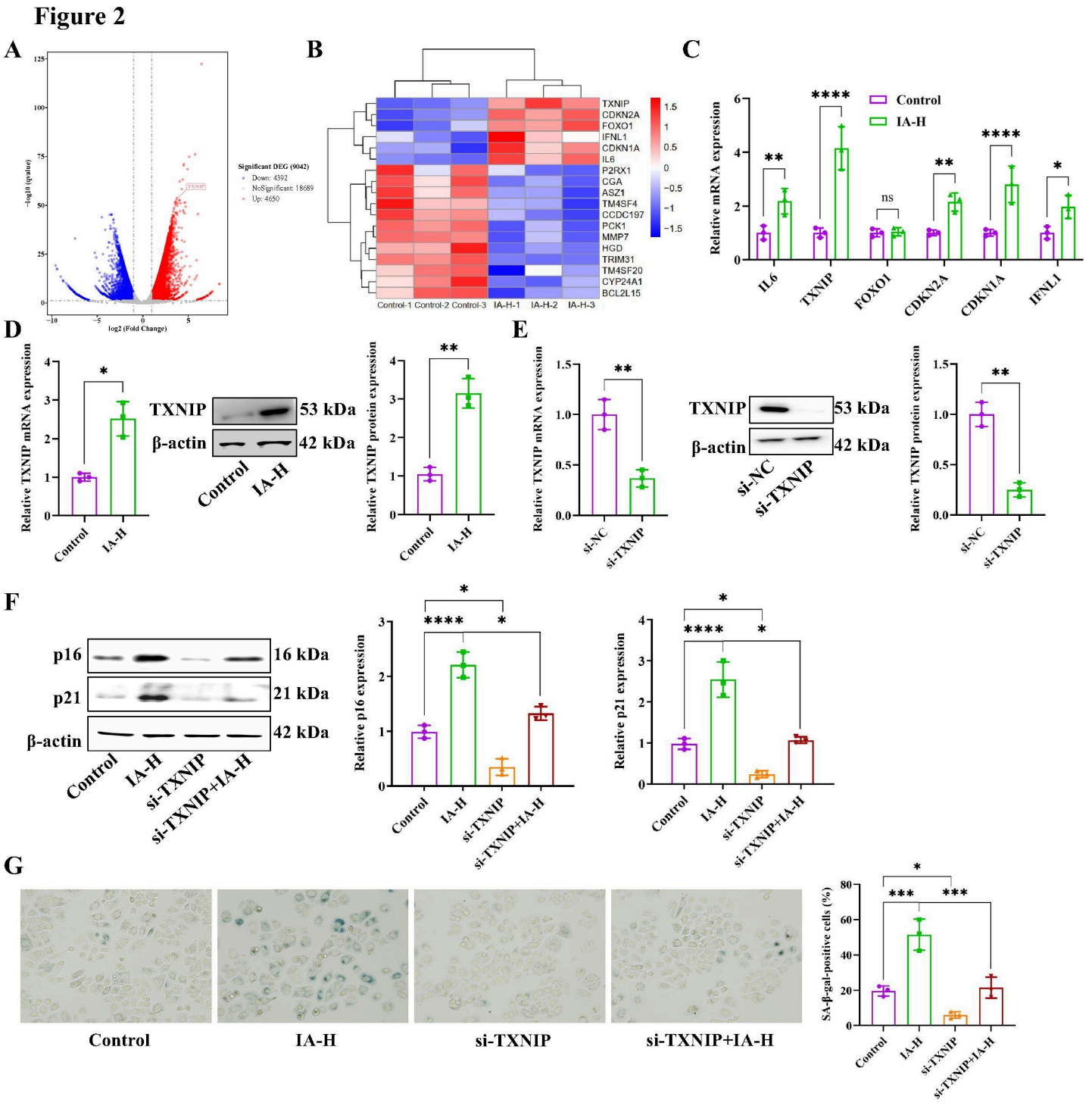


Figure 2

IA stimulates NCI-H460 cell senescence in a TXNIP-dependent manner.

(A) Volcano plot of RNA-seq analysis between IA-H group and control group. (B) Heatmap showing the significantly regulated genes measured in RNA-seq. (C) qRT-PCR analysis of six upregulated genes in heatmap. (D) Both qRT-PCR and western blotwere used to detect TXNIP expression in NCI-H460

cellschallenged with IA (40 mM) for 24 h. (E) The qRT-PCR and western blot analyses of TXNIP expression in NCI-H460 cells transfected with si-NC or si-TXNIP for 24 h. (F) NCI-H460 cells were transfected with si-TXNIP for 48 h and then treated with IA (40 mM)for another 24 h. Western blot was employed to determine p21 and p16 expression. (G) Representative SA-b-Gal staining images and quantification of positive-stained cells (scale bar=100 mm). Data shown are mean ± SD. *P < 0.05, **P < 0.01, ***P < 0.001, ****P < 0.0001, ns: not significant.

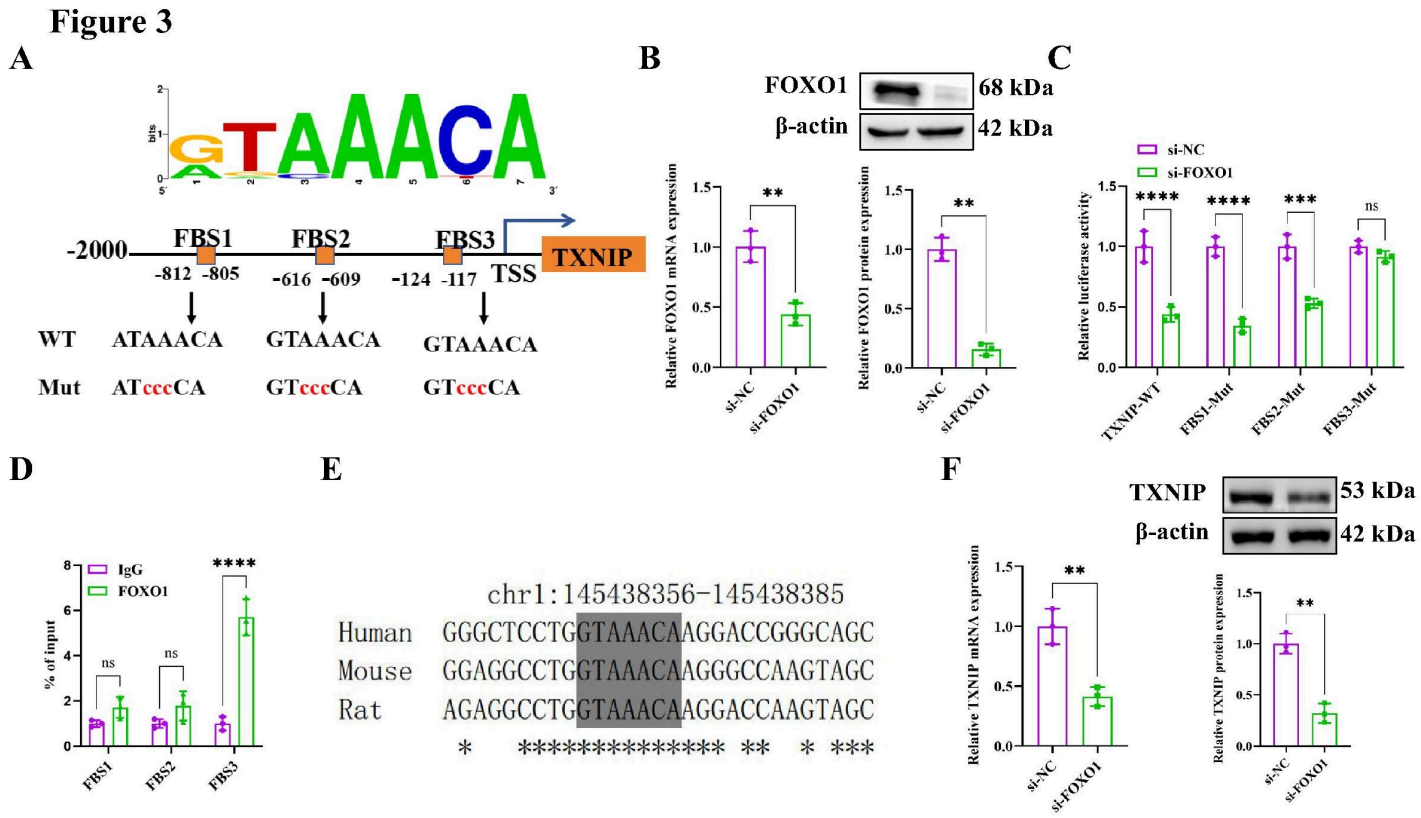


Figure 3

FOXO1 transcriptionally activates TXNIP.

(A) Predicted FOXO1sequence logo and the binding sites of FOXO1 in the TXNIP promoterby the JASPAR database, along with corresponding mutations. (B) qRT-PCR and western blot analyses of FOXO1 expression in NCI-H460 cells transfected with si-NCor si-FOXO1 for 48 h. (C) The luciferase reporter plasmids (FOXO1-WT, FBS1-Mut, FBS2-Mut or FBS3-Mut) were cotransfected into 293T cells with si-NC or si-FOXO1 for 48 h, followed by detection of luciferase activity. (D) DNA fragments containing FBS1, FBS2 or FBS3 were immunoprecipitated with FOXO1-specific antibody or IgG in NCI-H460 cells for ChIP-qPCR analysis. (E) Nucleotide sequence of FBS3 in various species, including human, mouse and rat. The conservation is shown in dark star. (F) Detection of TXNIP expression using qRT-PCR and western

blot in NCI-H460 cells transfected with si-NC or si-FOXO1 for 24 h. Data represent the mean ± SD from three independent experiments. **P < 0.01, ***P < 0.001, ****P < 0.0001, ns: not significant.

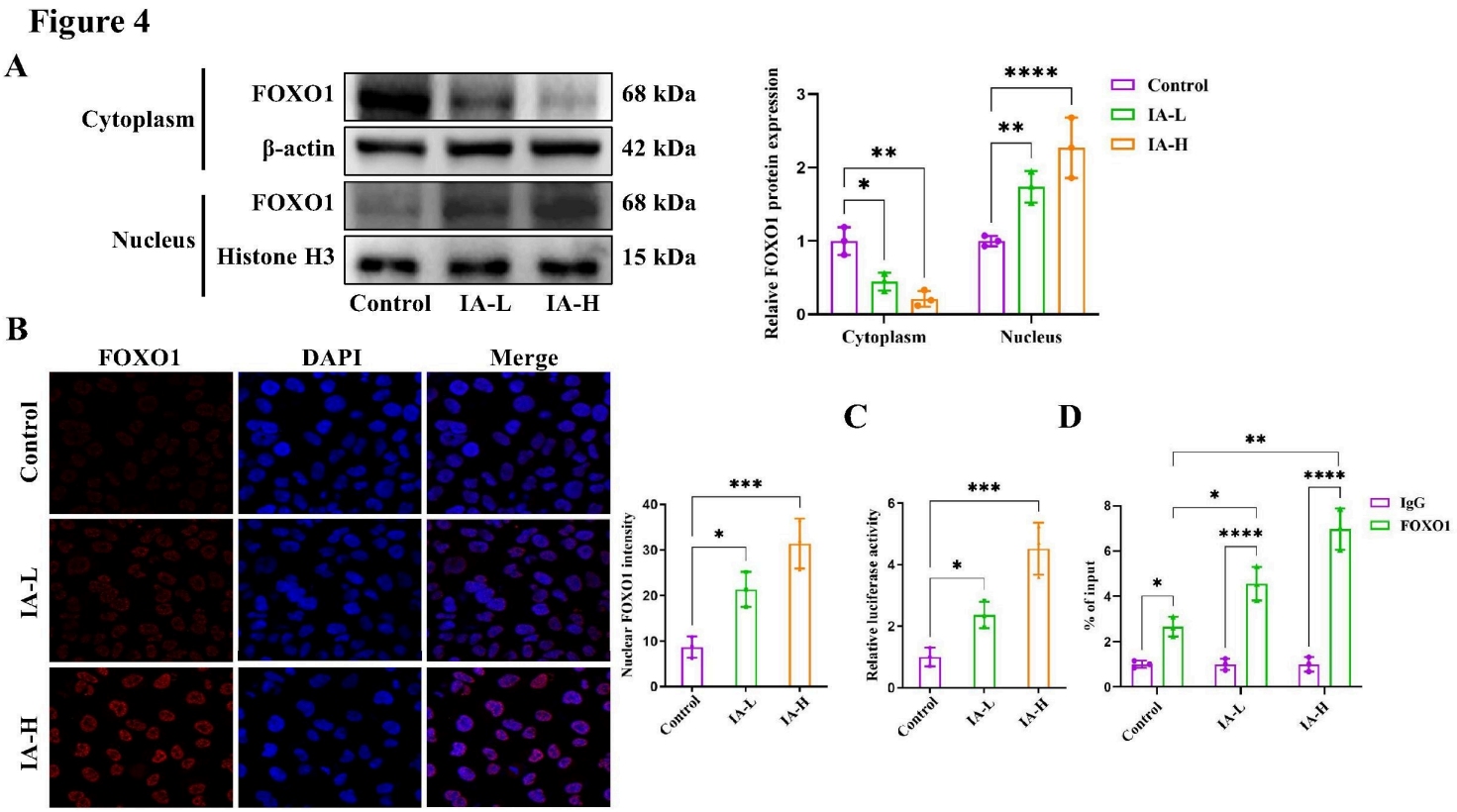


Figure 4

Effect of IA on FOXO1 nuclear translocation and TXNIP transcription.

(A) Western blot analysis of FOXO1 protein expression in the cytoplasm and nucleus of NCI-H460 cells incubated with 20 or 40 mM of IA for 24 h. (B) Representative pictures of immunofluorescence staining and quantification of nuclear FOXO1 intensity. (C) Luciferase activity of the TXNIP promoter in 293T cells treated with 20 or 40 mM of IA for 24 h. (D) ChIP-qPCR analysis for the binding of FOXO1 to the TXNIPpromoter containing the FBS3. All results are expressed as the mean ± SD from three independent experiments. *P < 0.05, **P < 0.01, ***P < 0.001, ****P < 0.0001.

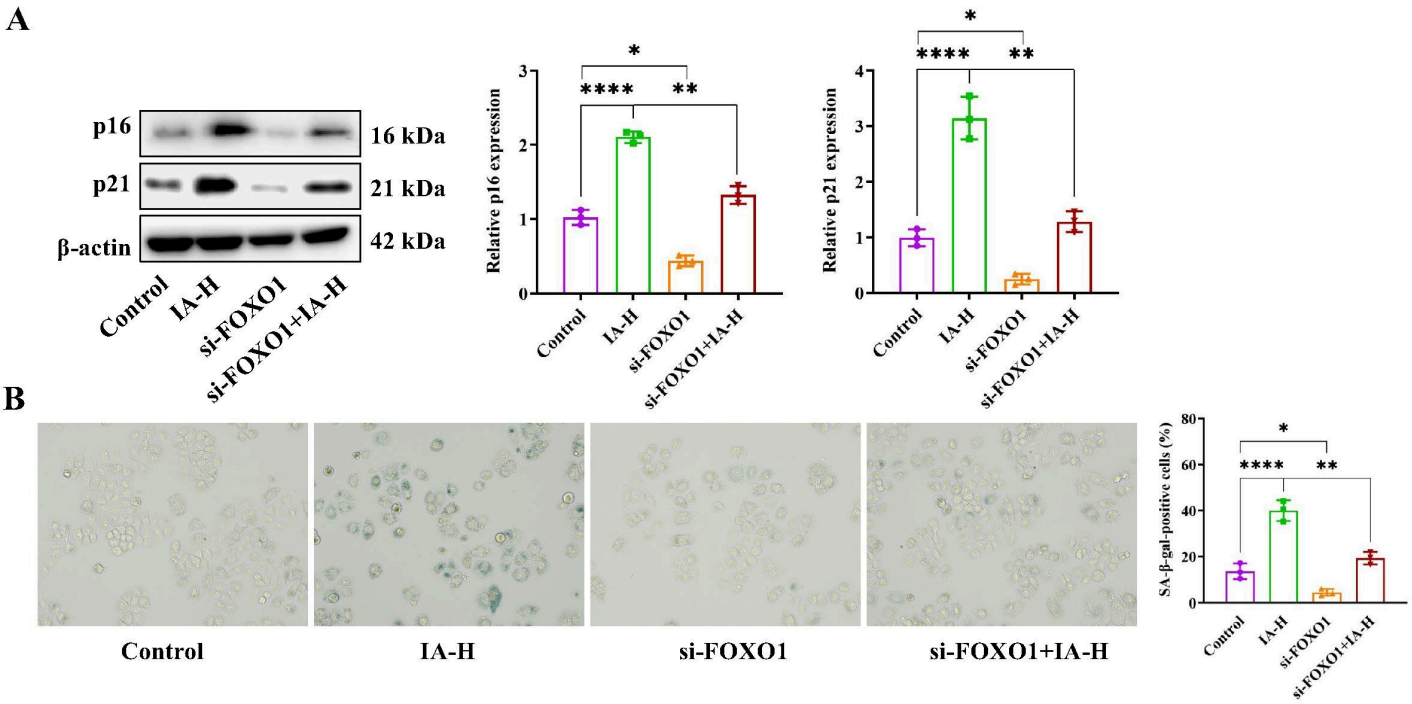


Figure 5

Involvement of FOXO1 in IA-induced NCI-H460 cell senescence.

(A) NCI-H460 cells were transfected with si-FOXO1 for 48 h, followed by treatment with 40 mM IA for an additional 24 h. Western blot was employed to measure the expression of p21 and p16. (B) Representative SA-b-Gal staining images and quantification of positive-stained cells. All results are expressed as the mean ± SD from three independent experiments. *P < 0.05, **P < 0.01, ****P < 0.0001.

Figure 6

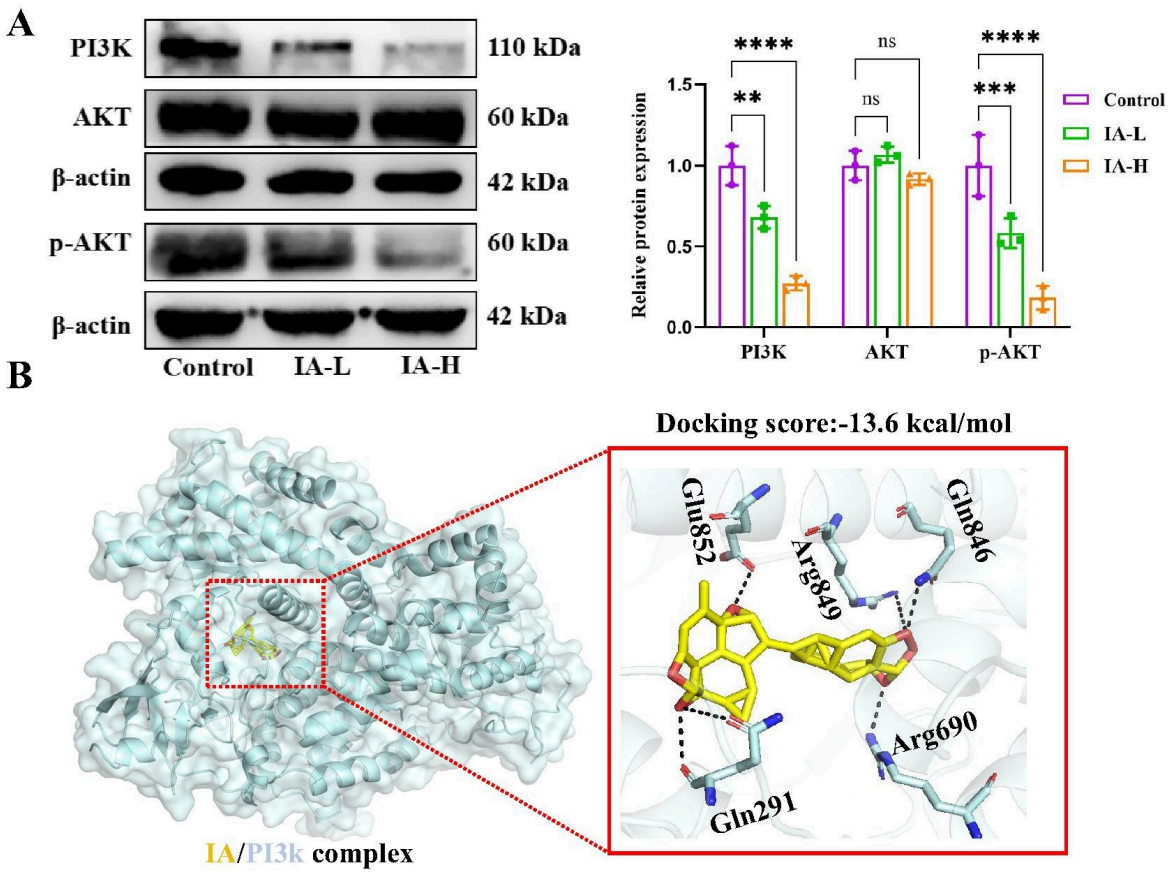


Figure 6

Effect of IA on the PI3K/Aktsignaling pathway.

(A) After treatment of NCI-H460 cells with 20 or 40 mM IA for 24 h, western blot was applied to detect PI3K expression and Akt phosphorylation. (B) Molecular docking model of IA versus PI3K.The results are shown as the mean ± SD. ***P* < 0.01, ****P* < 0.001,*****P* < 0.001, ns: not significant.

Figure 7

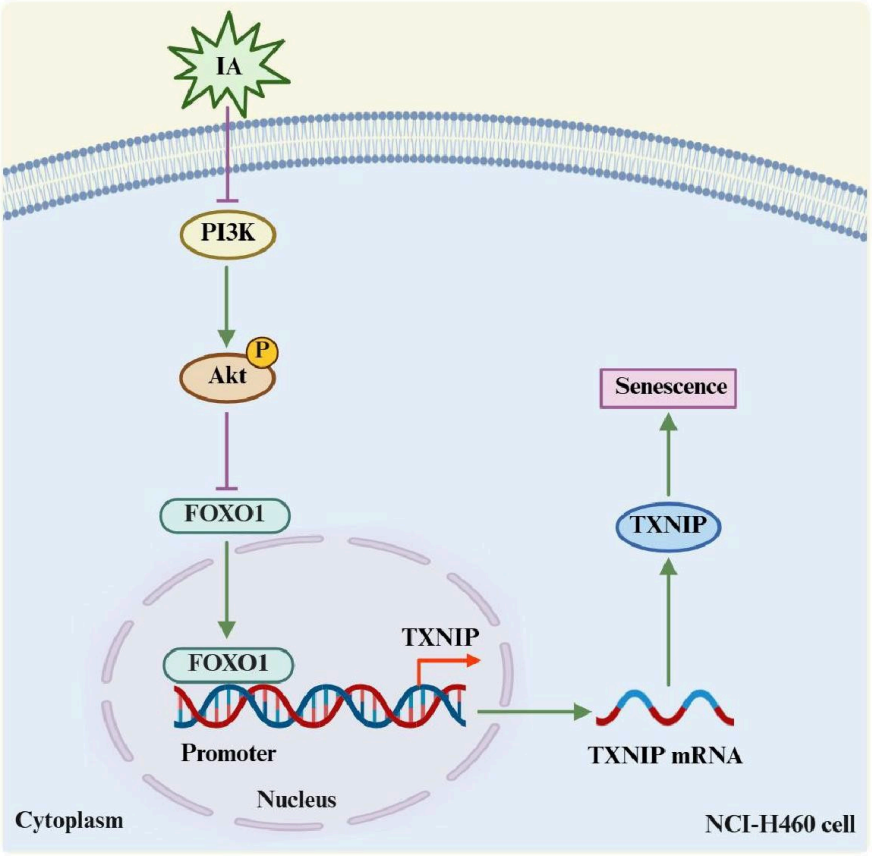


Figure 7

Schematic diagram of IA-induced NCI-H460 cell senescence.

IA inhibits the PI3K/Akt signaling pathway, leading to nuclear translocation of FOXO1. Nucleus accumulation of FOXO1 transcriptionally activates TXNIP and then induces NCI-H460 cell senescence. P:phosphorylation.

Supplementary Files

This is a list of supplementary files associated with this preprint. Click to download.

- Originalwesternblotimages.pdf